Research Article | Vol. 31, No. 11 / 22 May 2023 / Optics Express 18399
Optics EXPRESS

Hard X-ray stereographic microscopy for single-shot differential phase imaging

VALERIO BELLUCCI,[1] MARIE-CHRISTINE ZDORA,[2,3] LADISLAV MIKEŠ,[1] ŠARLOTA BIRNŠTEINOVÁ,[1] PETER OBERTA,[4,5] MARCO ROMAGNONI,[6] ANDREA MAZZOLARI,[6] PABLO VILLANUEVA-PEREZ,[7] RAJMUND MOKSO,[8] CHRISTIAN DAVID,[2] MIKAKO MAKITA,[1] SILVIA CIPICCIA,[9,10] JOZEF ULIČNÝ,[9,11] ALKE MEENTS,[12] ADRIAN P. MANCUSO,[1,13] HENRY N. CHAPMAN,[12,14,15] AND PATRIK VAGOVIČ[1,12,*]

[1]*European XFEL, Holzkoppel 4, 22869 Schenefeld, Germany*
[2]*Paul Scherrer Institute, Forschungsstrasse 111, 5232 Villigen PSI, Switzerland*
[3]*Institute for Biomedical Engineering, ETH Zürich, 8092 Zurich, Switzerland*
[4]*Institute of Physics, Academy of Sciences of the Czech Republic v.v.i., Na Slovance 2, 182 21, Praha 8, Czech Republic*
[5]*Rigaku Innovative Technologies Europe s.r.o., Novodvorská 994, 142 21, Praha 4, Czech Republic*
[6]*INFN Sezione di Ferrara, Via Saragat 1, 44122 Ferrara, Italy*
[7]*Synchrotron Radiation Research and NanoLund, Lund University, Box 118, 221 00, Lund, Sweden*
[8]*DTU Physics, Fysikvej, 310, 028 2800 Kgs. Lyngby, Denmark*
[9]*Diamond Light Source, Harwell Science and Innovation Campus, Didcot, Oxfordshire OX11 0DE, UK*
[10]*Department of Medical Physics and Biomedical Engineering, University College London, Gower Street, London WC1E 6BT, United Kingdom*
[11]*Faculty of Science, Department of Biophysics, P. J. Šafárik University, Jesenná 5, 04154 Košice, Slovakia*
[12]*Center for Free-Electron Laser Science CFEL, Deutsches Elektronen-Synchrotron DESY, Notkestr. 85, 22607 Hamburg, Germany*
[13]*Department of Chemistry and Physics, La Trobe Institute for Molecular Science, La Trobe University, Melbourne, Victoria 3086, Australia*
[14]*The Hamburg Centre for Ultrafast Imaging, Luruper Chaussee 149, 22761 Hamburg, Germany*
[15]*Department of Physics, Universität Hamburg, Luruper Chaussee 149, 22761 Hamburg, Germany*
[*]*patrik.vagovic@desy.de*

Abstract: The characterisation of fast phenomena at the microscopic scale is required for the understanding of catastrophic responses of materials to loads and shocks, the processing of materials by optical or mechanical means, the processes involved in many key technologies such as additive manufacturing and microfluidics, and the mixing of fuels in combustion. Such processes are usually stochastic in nature and occur within the opaque interior volumes of materials or samples, with complex dynamics that evolve in all three dimensions at speeds exceeding many meters per second. There is therefore a need for the ability to record three-dimensional X-ray movies of irreversible processes with resolutions of micrometers and frame rates of microseconds. Here we demonstrate a method to achieve this by recording a stereo phase-contrast image pair in a single exposure. The two images are combined computationally to reconstruct a 3D model of the object. The method is extendable to more than two simultaneous views. When combined with megahertz pulse trains of X-ray free-electron lasers (XFELs) it will be possible to create movies able to resolve 3D trajectories with velocities of kilometers per second.

#492137 https://doi.org/10.1364/OE.492137
Journal © 2023 Received 4 Apr 2023; revised 5 May 2023; accepted 9 May 2023; published 16 May 2023

Optics EXPRESS

1. Introduction

Multi-projection X-ray microscopy methods provide important technological advancements for the visualization of fast stochastic processes. In the so-called single-shot multi-projection approach, a sample is held fixed in an X-ray probe beam, and volume information is obtained simultaneously in several defined directions without the need for scanning or rotating the sample. In the hard X-ray regime, multiple projections can be obtained simultaneously using crystal beam splitters. These optical elements split the primary beam into multiple directions as shown schematically in Fig. 1. When a sample that is smaller than the width of the beam is inserted just downstream of the splitter it is illuminated from multiple directions, providing access to 3D information in a single-shot exposure. Recently, various beam-splitting schemes for monochromatic or broadband X-ray beams have been proposed and experimentally demonstrated at synchrotron radiation facilities [1–4]. These use Laue or Bragg diffraction geometries in crystals to generate multiple X-ray probes. Such approaches are suitable for recording multiple projection images in a single-pulse exposure at an XFEL source [5]. With the megahertz pulse trains available at the European XFEL, it becomes possible to far exceed the current capabilities of standard tomographic methods where the sample is rapidly rotated in the beam. The highest speed in tomography reported so far is 208 tomographic frames per second [6]. Increasing these speeds is not only technologically challenging but may affect the dynamics of the samples due to the strong centrifugal forces induced by fast sample rotation.

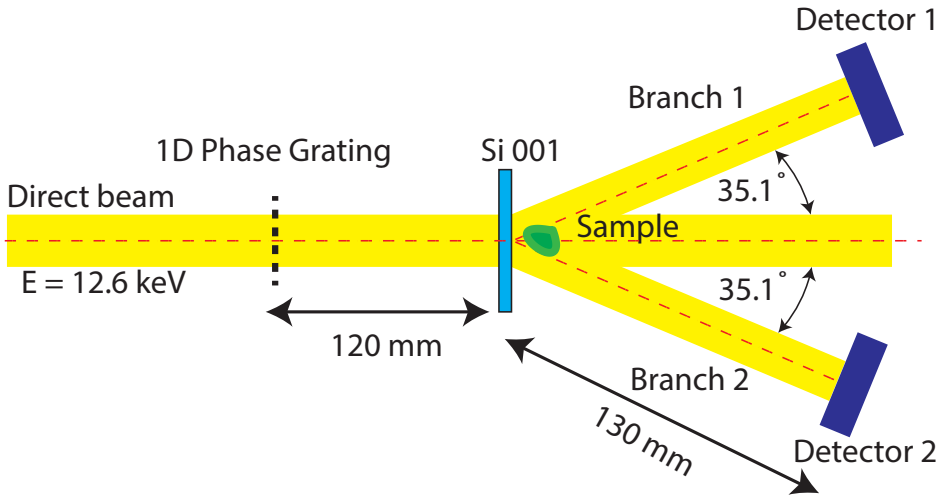

Fig. 1. Schematic diagram of the stereographic X-ray phase imaging method, using a single phase grating made from diamond and a Si 001 crystal splitter. The −1−3 1 and 1 3 1 reflections of the crystal beam-splitter were used to produce two identical X-ray beams. The sample was placed in the overlap region of the beams just after the splitter and two X-ray interferograms were recorded simultaneously at the two detectors, at two different views. The angle between the two views was 70.2°.

X-ray multi-projection imaging to date has mainly relied upon contrast generated by the propagation of the spatially coherent beam passing through the sample. That is, a near-field hologram or Fresnel diffraction of the object is recorded. For a pure phase object, the intensity in such an image is proportional to the Laplacian of the phase [7] and is thus sensitive to sharp transitions in density, e.g. at object boundaries, at the expense of smooth density variations in the sample. However, the characterization of many fast processes, such as shock wave propagation or mixing of fluids, requires tracking and quantifying smooth changes in density. Phase-contrast

Optics EXPRESS

imaging methodologies with the requisite sensitivity to these lower spatial frequencies exist that sense the first derivative of the phase. Many of these so-called differential phase-contrast methods utilize structures placed in the beam to modify the phase of the incident wavefront and are thus compatible with a single-shot acquisition. Among the many deterministic differential phase methods in the hard X-ray region, the most practical are based on periodic [8,9] or random phase modulators [10,11]. X-ray grating interferometry [12,13] has found broad application and is the method used here. The required phase gratings can be fabricated with high precision from low absorbing materials such as diamond [14] and which can withstand the high photon fluences of XFEL beams. Several single-shot schemes for phase-contrast imaging and wavefront sensing using a single phase grating have recently been demonstrated [8,9,15,16].

In this work, we combine multi-projection microscopy (in this case stereography) [3] with single-grating interferometry to show the feasibility of single-exposure stereographic X-ray phase-contrast imaging of a static phantom object. We placed the phase grating upstream of the beam-splitter so that it functions equivalently for all projections. We propose that this method can be applied at XFEL sources where it will enable time-resolved quantitative and highly sensitive phase imaging of fast stochastic processes. At the European XFEL, for example, imaging frame rates of up to several megahertz can be achieved [17].

2. Experimental

Our experiments were carried out at the Diamond Light Source (UK) high-coherence beamline I13-1 [18]. The photon energy was set to 12.6 keV using a horizontal two-bounce Si 111 monochromator. A linear diamond transmission phase grating with a pitch of 4 μm and structure height of 3.8 μm was placed in front of the thin Si crystal beam-splitter. The diffraction vectors (+1 and −1 orders) of the phase grating were oriented in the vertical plane, perpendicular to the diffraction plane of the splitter to avoid Fourier filtering of the diffracted waves from the grating by narrow angular acceptance of the splitter in the diffraction plane. The splitter was produced in the laboratories of INFN-Ferrara (Italy) by anisotropic etching of an area of 5 mm × 5 mm into a 500 μm thick wafer to leave a 30 μm thick single-crystal membrane supported by a frame. The normal of the main face of the splitter coincides with the (001) crystallographic direction and the sides of the square membrane are parallel to the (0-10) and (001) directions. X-rays passing through a crystal generate a diffracted beam for every lattice plane that is oriented such that its Bragg diffraction condition is obeyed. The symmetries of families of planes can be exploited for selecting multiple planes that diffract at the same Bragg angle and specific photon energy to generate several beams with equal efficiency. The 113 family of planes was used in this experiment, following earlier practice [3]. The included angle between the (001) direction and the reciprocal lattice point of any of the eight reflections in this family is 17.55° and thus the diffraction condition is satisfied for a beam incident in the 100 direction with a wavelength commensurate with the 17.55° Bragg angle. We used the −1−3 and 1 3 1 reflections for the two projection imaging branches. These lie in a plane that is tilted by $\arctan 1/3 = 18.4°$ to the 001 plane. The splitter was therefore rotated around the beam axis by this angle to place these two diffracted beams in the horizontal diffraction plane (Fig. 1). The angle between the two chosen beams is 70.2°. The splitter was slightly de-tuned to excite only two diffraction waves in a horizontal plane from −1−3 1 and 1 3 1 reflections rather than all 8 waves from the 113 family. The sample was placed approximately 0.6 mm downstream of the splitter in the beam overlap region so that it was illuminated simultaneously by the diffracted beams as well as the transmitted beam. The direct transmitted beam, which also illuminated the sample, was not used in this case due to the lack of a third X-ray detector. The sample consisted of soda lime glass spheres with a diameter of 100 μm glued onto a bundle of carbon fibres. Two simultaneous X-ray projection interferometric images were recorded using high-resolution indirect X-ray detectors. two high-resolution indirect-detection X-ray microscopes. Each microscope was composed of a

Optics EXPRESS

scintillator coupled via diffraction-limited optics to a CCD detector (PCO4000, 4008 × 2672 pixels, 9 μm pixel size). A total magnification of 20x was used in the experiment, providing an effective pixel size of 0.45 μm. An exposure time of 5 s was used. A photograph of the experimental setup is shown in Fig. 2.

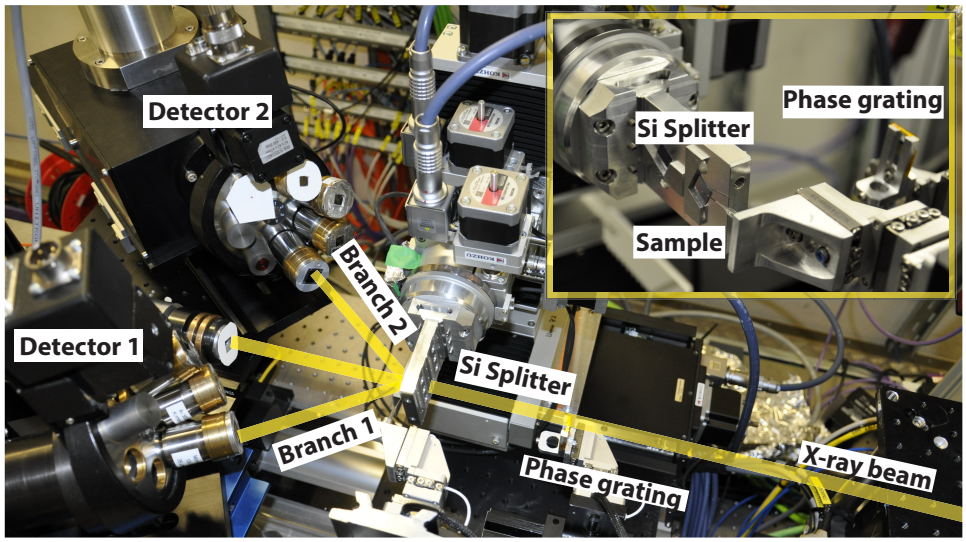

Fig. 2. Photograph of the set-up during the experiment at the Diamond Light Source I13 coherence branch beamline, showing the beam paths. The insert shows details of the grating, crystal beam-splitter, and sample.

3. Results and discussion

The recorded interferograms were processed using the Fourier method [19,20] to extract the phase gradient and absorption images. Absorption images were obtained from zero order peak in the Fourier domain (DC component) and successive inverse Fourier transform. The phase gradient images were obtained by isolation of the first-order peak in the Fourier domain and its shift to zero frequency position. After the inverse Fourier transform, the differential phase image was obtained in the spatial domain followed by integration to obtain the phase map. The results are shown in Fig. 3. The phase profiles obtained from the two branches match well with the theoretical phase profiles of lime glass spheres.

Further, we reconstructed a 3D model of the sample using a stereographic point-based technique [21–23]. This relies on finding low-level primitives or features of the object that can be unambiguously identified in several of the multi-view images. As an example, it is possible to fit circles to the borders of the projections of the glass spheres to locate their centers by triangulation. We consider a coordinate system for the model where Z is in the direction of the incident beam, Y is vertical, and X horizontal. The two projections are labeled 1 and 2, with direction cosines in the Z direction of $\cos\alpha$ and opposite X components (here, $\alpha = 35.1°$, see Fig. 1). Under the assumption that the projections are formed with collimated beams, the Y coordinate of a sphere is the same in the two projections: $Y = Y_1 = Y_2$. A sphere is identified in the two projections at positions x_1 and x_2 (in the rotated coordinate systems of those projections), giving rays at positions $X_{1P} = x_1/\cos\alpha + X_{10}$ and $X_{2P} = x_2/\cos\alpha + X_{20}$ in the global coordinate system, where X_{10} and X_{20} give the origins of the two projection images in global coordinates. The global X and

Optics EXPRESS

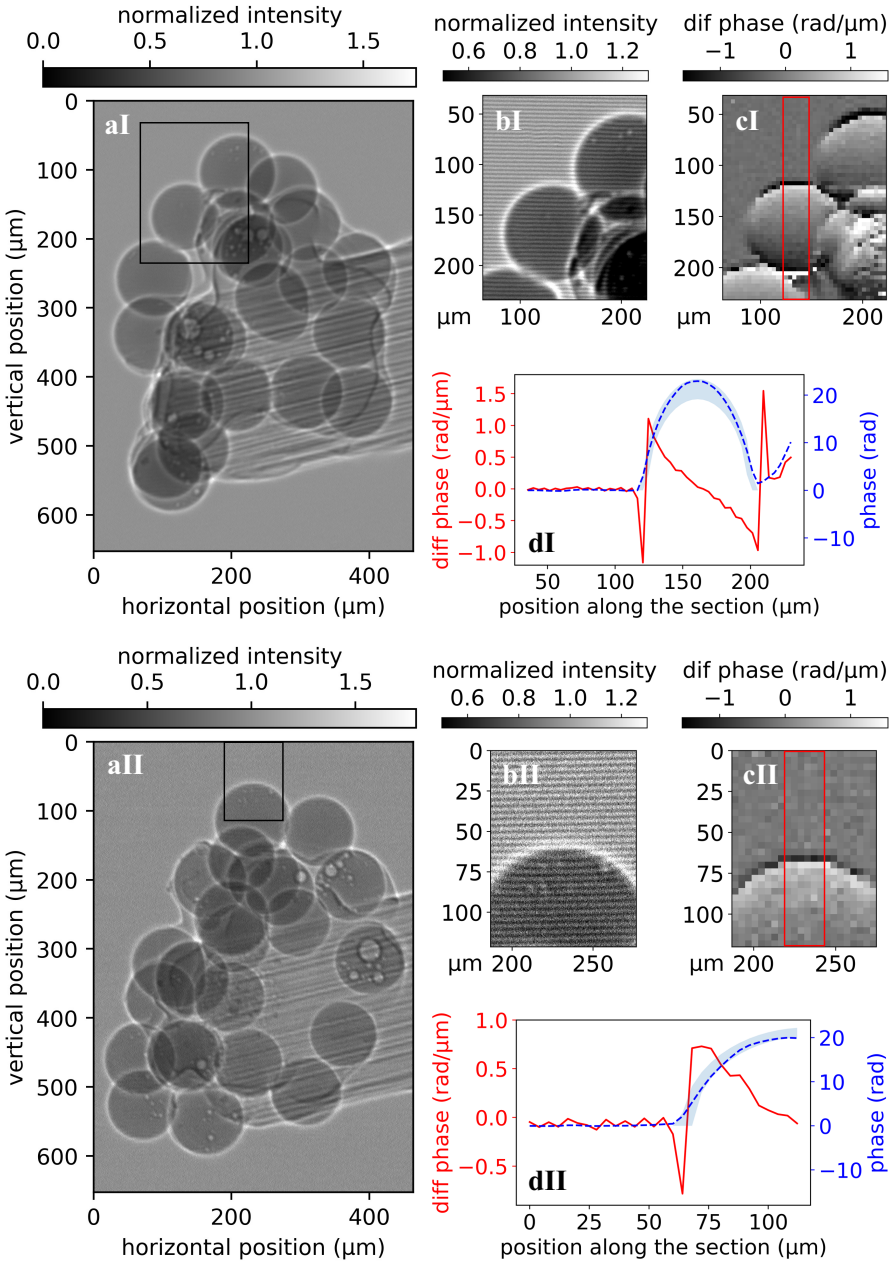

Fig. 3. (aI, aII) Absorption images for branches 1 and 2. (bI, bII) Raw interferograms for the black rectangle in panels (aI) and (aII), respectively for branch 1 (bI) and branch 2 (bII). (cI, cII) Differential phase image reconstructed from the interferograms in the region of the black rectangle shown in panels (aI) and (aII), respectively for branch 1 (cI) and branch 2 (cII). (dI, dII) Comparison of the extracted differential phase (continuous red line), integrated phase (dashed blue line) and theoretically expected phase (blue shade) of the lime-glass spheres with a diameter of 100 µm including thickness tolerance given by the manufacturer. The experimental plots represent an average over the columns in the red rectangles in panels (cI) and (cII).

Optics EXPRESS

Z coordinates of the sphere can then be determined by finding intersections of rays described as

$$X = \tan(\alpha)\, Z + X_{1P} \tag{1}$$

and

$$X = \tan(-\alpha)\, Z + X_{2P}. \tag{2}$$

Equating these gives a solution for the intersection at

$$Z_i = (X_{2P} - X_{1P})/(2\tan(\alpha)) \tag{3}$$

$$X_i = (X_{2P} + X_{1P})/2. \tag{4}$$

This solution can be applied to any pair of points in the two projections that are identified with the same object, to locate that object in three dimensions. This was carried out for the centers of the spheres and some identifiable features of the carbon fibres. The two branches differ in the position of the sample illumination, but this does not affect the 3D reconstructed image. This difference produces just a horizontal translation of the 2D images over the field-of-view of the camera. This effect is indistinguishable from a translation of the cameras, so it is accounted for within the treatment of the positioning errors of the cameras. This translation does not affect the 3D reconstructed image since its only effect is a translation of the entire 3D image in the 3D

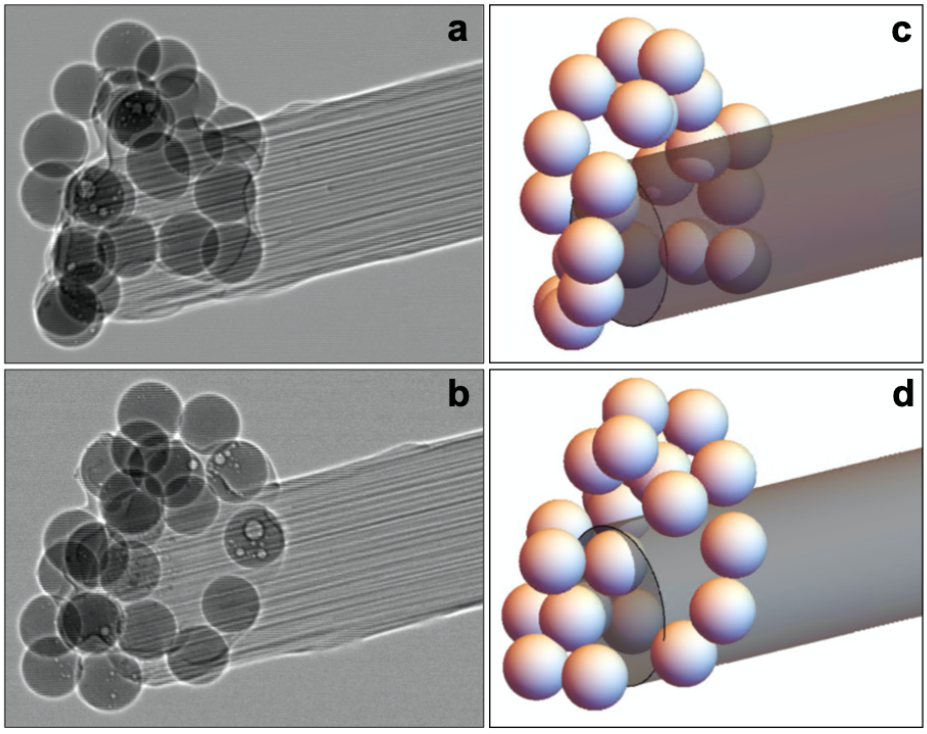

Fig. 4. Stereographic images of the sample with projection angle +35.1° (a) and −35.1° (b). 3D reconstruction of the sample as seen from these observation angles (c,d). The carbon fiber filament is approximated to a cylinder to increase its transparency so to ease the identification of the spheres The soda-lime glass spheres are non-intersecting and separated from the structure of the carbon fibre thread, composed of a multitude of micrometer fibres (The 3D volume can be seen under various views rendered in the video in Visualization 1).

Optics EXPRESS

space, which is eliminated by shifting the axis origin. The result of the reconstructed model is shown in Fig. 4, which is plausible since none of the spheres are overlapping with each other or the fibre bundle. This approach relies upon unambiguously identifying pairs of points in the two projections, which is not always possible. Nevertheless, it may provide a model that is a good enough starting point for further refinement through statistical methods [24], which was not performed in this work.

4. Conclusions

In summary, we have successfully demonstrated combining phase imaging using grating interferometry with stereographic image acquisition, to provide a way to obtain three-dimensional structural information in a single shot. From the simultaneously recorded interferograms, the phase information was recovered and the 3D information was accurately obtained. We propose to use this method for stereographic or multi-projection microscopy at megahertz XFEL sources for the visualization of complex dynamic phenomena in three dimensions, such as liquid mixing or shock-wave propagation. It should be noted that the proposed method has limitations that need to be addressed and investigated in order to achieve a practical implementation at XFEL sources. The most significant is the photon energy acceptance of the splitter crystal, which limits the spectral bandwidth of the diffracted beams and fixed photon energy in the case of multi-wave excitation. The loss of flux outside this bandwidth could be reduced by generating pulses of narrower bandwidth to begin with, as are obtained by seeded SASE beams [25]. However, these issues could be mitigated by employing other splitter schemes that are tunable in photon energy and projection angle.

Funding. HORIZON EUROPE European Innovation Council (101046448); Deutsche Forschungsgemeinschaft (EXC 2056, project ID 39071599); Vetenskapsrådet (2017-06719); Bundesministerium für Bildung und Forschung (05K18XXA).

Acknowledgments. Beamtime was granted at Diamond Light Source beamline I13 in the frame of proposal MT17739.

Disclosures. The authors declare no conflicts of interest.

Data availability. Data underlying the results presented in this paper are not publicly available at this time but may be obtained from the authors upon reasonable request.

References

1. M. Hoshino, K. Uesugi, J. Pearson, T. Sonobe, M. Shirai, and N. Yagi, "Development of an x-ray real-time stereo imaging technique using synchrotron radiation," J. Synchrotron Radiat. **18**(4), 569–574 (2011).
2. R. Mokso and P. Oberta, "Simultaneous dual-energy X-ray stereo imaging," J. Synchrotron Radiat. **22**(4), 1078–1082 (2015).
3. P. Villanueva-Perez, B. Pedrini, R. Mokso, P. Vagovic, V. A. Guzenko, S. J. Leake, P. R. Willmott, P. Oberta, C. David, H. N. Chapman, and M. Stampanoni, "Hard x-ray multi-projection imaging for single-shot approaches," Optica **5**(12), 1521–1524 (2018).
4. W. Voegeli, K. Kajiwara, H. Kudo, T. Shirasawa, X. Liang, and W. Yashiro, "Multibeam x-ray optical system for high-speed tomography," Optica **7**(5), 514–517 (2020).
5. K. E. Schmidt, J. C. H. Spence, U. Weierstall, R. Kirian, X. Wang, D. Starodub, H. N. Chapman, M. R. Howells, and R. B. Doak, "Tomographic femtosecond x-ray diffractive imaging," Phys. Rev. Lett. **101**(11), 115507 (2008).
6. F. García-Moreno, P. H. Kamm, T. R. Neu, F. Bülk, R. Mokso, C. M. Schlepütz, M. Stampanoni, and J. Banhart, "Using x-ray tomoscopy to explore the dynamics of foaming metal," Nat. Commun. **10**(1), 3762 (2019).
7. K. A. Nugent, D. Paganin, and T. E. Gureyev, "A phase odyssey," Phys. Today **54**(8), 27–32 (2001).
8. Y. Takeda, W. Yashiro, Y. Suzuki, S. Aoki, T. Hattori, and A. Momose, "X-ray phase imaging with single phase grating," Jpn. J. Appl. Phys. **46**(3), L89–L91 (2007).
9. W. Yashiro, Y. Takeda, A. Takeuchi, Y. Suzuki, and A. Momose, "Hard-x-ray phase-difference microscopy using a fresnel zone plate and a transmission grating," Phys. Rev. Lett. **103**(18), 180801 (2009).
10. S. Berujon, H. Wang, and K. Sawhney, "X-ray multimodal imaging using a random-phase object," Phys. Rev. A **86**(6), 063813 (2012).
11. K. S. Morgan, D. M. Paganin, and K. K. W. Siu, "X-ray phase imaging with a paper analyzer," Appl. Phys. Lett. **100**(12), 124102 (2012).

Optics EXPRESS

12. C. David, B. Nöhammer, H. H. Solak, and E. Ziegler, "Differential x-ray phase contrast imaging using a shearing interferometer," Appl. Phys. Lett. **81**(17), 3287–3289 (2002).
13. A. Momose, S. Kawamoto, I. Koyama, Y. Hamaishi, K. Takai, and Y. Suzuki, "Demonstration of x-ray talbot interferometry," Jpn. J. Appl. Phys. **42**(Part 2, No. 7B), L866–L868 (2003).
14. M. Makita, P. Karvinen, V. Guzenko, N. Kujala, P. Vagovic, and C. David, "Fabrication of diamond diffraction gratings for experiments with intense hard x-rays," Microelectron. Eng. **176**, 75–78 (2017). Micro- and Nano-Fabrication.
15. S. Matsuyama, H. Yokoyama, R. Fukui, Y. Kohmura, K. Tamasaku, M. Yabashi, W. Yashiro, A. Momose, T. Ishikawa, and K. Yamauchi, "Wavefront measurement for a hard-X-ray nanobeam using single-grating interferometry," Opt. Express **20**(22), 24977 (2012).
16. M. Seaberg, R. Cojocaru, and S. Berujon, *et al.*, "Wavefront sensing at X-ray free-electron lasers," J. Synchrotron Radiat. **26**(4), 1115–1126 (2019).
17. P. Vagovič, T. Sato, and L. Mikeš, *et al.*, "Megahertz x-ray microscopy at x-ray free-electron laser and synchrotron sources," Optica **6**(9), 1106–1109 (2019).
18. C. Rau, S. Marathe, A. J. Bodey, M. Storm, D. Batey, S. Cipiccia, P. Li, and R. Ziesche, "Operando and high-throughput multiscale-tomography," in *Developments in X-Ray Tomography XIII*, vol. 11840 B. Müller and G. Wang, eds., International Society for Optics and Photonics (SPIE, 2021), pp. 192–200.
19. M. Takeda, H. Ina, and S. Kobayashi, "Fourier-transform method of fringe-pattern analysis for computer-based topography and interferometry," J. Opt. Soc. Am. **72**(1), 156–160 (1982).
20. H. H. Wen, E. E. Bennett, R. Kopace, A. F. Stein, and V. Pai, "Single-shot x-ray differential phase-contrast and diffraction imaging using two-dimensional transmission gratings," Opt. Lett. **35**(12), 1932–1934 (2010).
21. Y. Abdel-Aziz, H. Karara, and M. Hauck, "Direct linear transformation from comparator coordinates into object space coordinates in close-range photogrammetry*," Photogramm. Eng. Remote Sens. **81**(2), 103–107 (2015).
22. B. André B, J. Dansereau, and H. Labelle, "Effect of radiographic landmark identification errors on the accuracy of three-dimensional reconstruction of the human spine," Med. Biol. Eng. Comput. **30**(6), 569–575 (1992).
23. L. C. Chen, C. W. Armstrong, and D. D. Raftopoulos, "An investigation on the accuracy of three-dimensional space reconstruction using the direct linear transformation technique," J. Biomech. **27**(4), 493–500 (1994).
24. J. A. Fessler, *Statistical Image Reconstruction Methods for Transmission Tomography* (SPIE, 2000), pp. 1–71.
25. G. Geloni, V. Kocharyan, and E. Saldin, "A novel self-seeding scheme for hard x-ray fels," J. Mod. Opt. **58**(16), 1391–1403 (2011).